communications chemistry

A Nature Portfolio journal

Article

https://doi.org/10.1038/s42004-025-01607-x

Emergence of conformational diversity and complexity of supramolecular structure by the interaction of a simple molecule with a uniform surface

S. Fatemeh Mousavi[1], Aisha Ahsan[1,2], Aaron Oechsle[1,2], Narmadha Devi[1,2], Yoshitaka Matsushita[3], Luiza Buimaga-Iarinca[4], Cristian Morari[4], Waka Nakanishi[5,6], Katsuhiko Ariga[7,8], Yutaka Wakayama[7], Yusuke Yamauchi[9,10,11], Thomas A. Jung[1,2] ✉ & Jonathan P. Hill[7] ✉

The emergence of complexity during self-assembly of simple molecular building blocks is an important aspect in the synthesis of nanoarchitectures from supramolecular functional units. In particular, two-dimensional nanostructures are important from the point-of-view of technological applications. Here, a remarkably complex on surface network is observed to form spontaneously from a single molecular module (porphyrin) having multiple site-specific conformations. The interplay of different physicochemical interactions at the surface contributes to the site-specific symmetry breaking of the porphyrin conformation, and was investigated at different substrates. Molecular conformational flexure, relocation in the corrugated surface potential, interactions with surface state electrons, and last but not least mutual intermolecular binding by hydrogen bonding at different elevations above the substrate are critical elements. We discuss the possibility of surfaces and interfaces causing quasidegeneracy of molecular configurations in supramolecular self-assembly, and the adsorbate-adsorbent interface as the driver for this system to behave counterintuitively to equilibrium thermodynamics.

The emergence of larger supramolecular systems is directly related to many possible applications and connotations for synthetic or preprogrammed control of functional (surface) materials. Prebiotic supramolecular systems may have included oscillatory chemical reactions and autocatalytic self-replicative molecular aggregates in the fluid (i.e. liquid or gas) phase, for example ref. 1,2. The air-water interface and related hydrophobic/hydrophilic interactions leading to colloidal aggregates including vesicles[3] and nanotubes[4] also present prime examples by which complexity can emerge based on programmed molecular design of the aggregating molecules. The important role of lipid vesicles and membranes in many biochemical processes and successful supramolecular assembly at solid surfaces[5] or within bilayers[6,7] attest to the importance of these processes, and the decisive role of supramolecular structures at membranes and phase boundaries[8], for metabolic activity[9], and molecular motors[10], including artificial molecular machines[11,12], provide further proof that complexity can be attained from few simple components.

The development or evolution of supramolecular assemblies as functional perhaps even self-replicating materials would be a significant advance

[1]Department of Physics, University of Basel, Basel, Switzerland. [2]Laboratory for Micro- and Nanotechnology, Paul Scherrer Institute, Villigen PSI, Switzerland. [3]Research Network and Facility Services Division, National Institute for Materials Science, Tsukuba, Japan. [4]National Institute for Research and Development of Isotopic and Molecular Technologies (NIRDIMT), Cluj-Napoca, Romania. [5]Molecular Design and Function Group, National Institute for Materials Science, Tsukuba, Japan. [6]Research Center for Autonomous Systems Materialogy (ASMat), Institute of Innovative Research, Tokyo Institute of Technology, Yokohama, Japan. [7]Research Center for Materials Nanoarchitectonics, National Institute for Materials Science, Tsukuba, Japan. [8]Department of Advanced Materials Science, Graduate School of Frontier Sciences, The University of Tokyo, Chiba, Japan. [9]Department of Materials Process Engineering, Graduate School of Engineering, Nagoya University, Nagoya, Japan. [10]Department of Chemical and Biomolecular Engineering, Yonsei University, Seoul, South Korea. [11]Australian Institute for Bioengineering and Nanotechnology (AIBN) and School of Chemical Engineering, The University of Queensland, Brisbane, QLD, Australia. ✉e-mail: thomas.jung@psi.ch; Jonathan.Hill@nims.go.jp

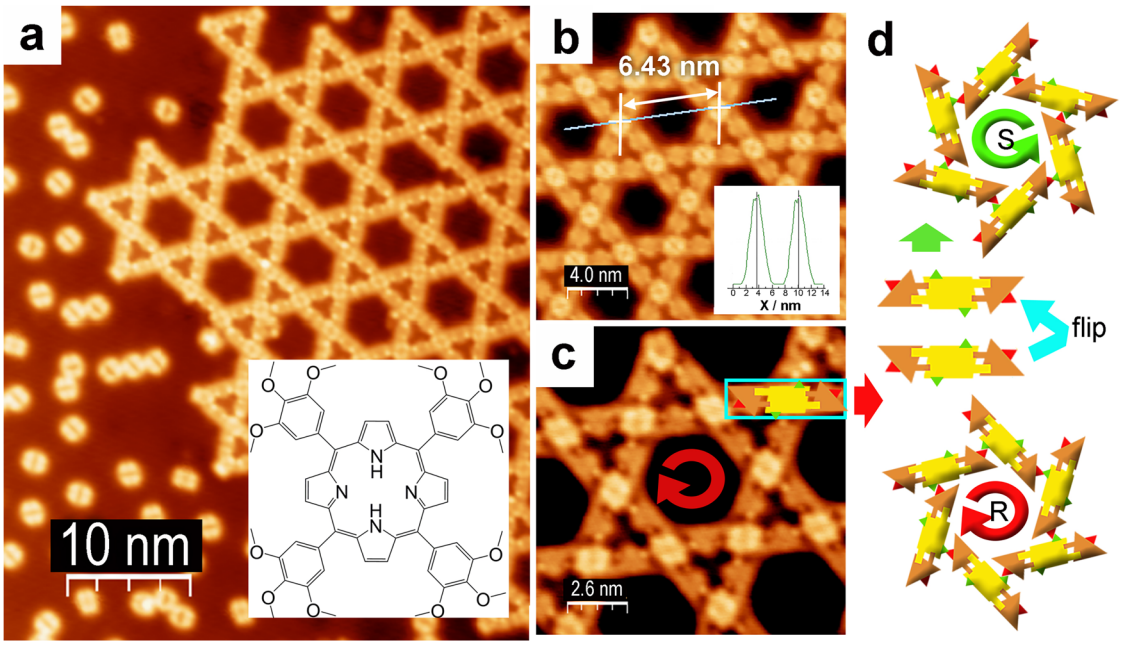

Fig. 1 | Chemical and self-assembled structure of TTMPP. a STM image of Kagome lattice formation of TTMPP on Ag(111) surface (Image: 50 nm; $I = 10$ pA; $V = 1.5$ V); inset: chemical structure of TTMPP. **b** STM image of Kagome structure at negative bias (π-imaging mode; image: 13 nm; $I = 30$ pA; $V = -200$ mV) showing the large (6.43 nm) pore formed by the Kagome lattice. **c** Positive bias STM image with a notional trimer of molecules highlighted to identify the chirality of the Kagome lattice. **d** Graphical representation of the molecular trimer composing the chiral Kagome structure, STM images contained in Fig. 1 have right-handed (R) planar chirality. See also Supplementary Fig. 2.

analogous with the complex biosystems that have evolved over geological time on Earth. For this advance to occur in synthetic systems, molecules need to be driven far out of their "in-fluid and thermodynamic equilibrium at low concentration" configuration[13]. The accumulation and assembly under entropic constraints, in this case, involves the formation of molecular modules driven by the adsorption energy at an interface and the concurrent intermolecular interactions. It is such considerations that motivate the investigation of the physicochemical origins of complexity involving simple molecular modules assembling cooperatively at model interfaces. In this work, we show a supramolecular structure possessing remarkable complexity, which emerges from the interactions of a single molecular building block due to its cooperative and ligand-site-specific interactions in a delicate balance of surface-molecule and inter-molecular forces. This structure formation is also accompanied by a remarkable conformational diversity.

In solution, a fluid matrix – most commonly water—is intimately involved in determining the outcome of self-assembly. At surfaces and interfaces the situation becomes significantly more complex in the sense that surface/interface potentials reduce the symmetry of the system and confine molecules within two dimensions and/or direct molecular orientations according to hydrophilic/hydrophobic interactions. For the present study, we have selected porphyrins as they can be equipped with application-specific functional groups derived from e.g., *meso*-tetraphenylporphyrin, TPP. The related compounds are archetypal molecules used to investigate self-assembly processes at interfaces[14–18] due to their appropriate dimensions and dimensionality (i.e., ∅ 1–2 nm, 2D form), and their excellent stability towards physical vapor deposition. These molecules are attractive not only from the point-of-view of their tunable self-assembly[19], but also because of the possibility of their conformational identification by scanning probe microscopy, when adsorbed on atomically clean surface substrates[20,21]. Beyond the programming of their supramolecular organization by ligand substitution, their electronic[22], optical[23], sensing[24] and catalytic properties[25] are also remarkable.

To investigate the onset of complexity in on-surface supramolecular organization in a suitable model system, we have chosen a moderately interacting ligand moiety: 3,4,5-trimethoxyphenyl groups can form intra- and intermolecular hydrogen bonds (H-bonds). 5,10,15,20-Tetrakis(3,4,5-trimethoxyphenyl)porphyrin (TTMPP, see inset Fig. 1a for chemical structure and Supplementary Fig. 1 for the solid state molecular structure) exhibits three conformational adaptations: i) the porphyrin plane is prone to bending or saddling in the surface potential as has been studied and reported by several authors[26–28], ii) the phenyl porphyrin bond can assume different dihedral angles enabling the formation of chiral and achiral conformers on surfaces, and iii) the 12 methoxy groups can sample a large conformational space as each of them can rotate around the axis of the phenyl-oxygen bond.

Here, we have analyzed the conformation of individual molecules in relation to their coverage dependent supramolecular organization on two selected solid substrates i.e. Ag(111) and Au(111). At lower surface coverages, Low Temperature Scanning Tunneling Microscopy (LT-STM) reveals single, non-interacting conformers, but as more material is deposited, molecules modify their conformations and configurations leading to the formation of a complex, chiral Kagome lattice. On the one hand, this transition is driven by intermolecular H-bonds formed between peripheral methoxy (-OCH_3) groups and molecule-surface interactions. On the other hand, the Kagome network topology is an alternative to the formation of compact supramolecular islands. While the sum of all intermolecular interactions in a compact 2D superstructure island is expectedly higher, the survival of the surface state in the form of a confined quantum well state in the pores fosters the presence of pores/network formation and repels adsorbates inside the pores.

Results and discussion

Structure

As shown in Supplementary Fig. 1, the X-ray crystal structure of TTMPP[29–31] contains 3,4,5-trimethoxyphenyl groups at its meso positions (between pyrrole groups), and these are non-coplanar with the porphyrin macrocycle subtending dihedral angles of 59° and 85° respectively with substituents at 5,15 and 10,20 positions. This indicates that these substituents are not fixed in nearly orthogonal orientation but that they can rotate in response to local constraints. The deposition under UHV conditions of TTMPP on a flat Ag(111) substrate leads unexpectedly to the formation of a Kagome lattice

structure (Fig. 1a) over large areas of substrate exceeding 100 nm^2. The lattice contains hexagonal pores (diameter 6.4 nm: Fig. 1b) and smaller triangular pores establishing the Kagome topology. The structure is chiral due to a six-fold propeller-like arrangement of molecular trimers forming the lattice (see Fig. 1c,d) as well as the unsymmetrical topography of the molecules represented as bright spots in the STM images (Fig. 1c,d; see also Supplementary Fig. 2 for examples of *R* and *S* structures). Other salient features of the structure include its relative lack of defects (i.e., vacancy sites in the network backbone are observed in less than 0.1% of the lattice sites. Also scarce guest molecules have been observed in the larger voids of the lattice (i.e., around 6% occupancy by possible molecules and/or ad-atoms). These observations indicate not only that adsorption of TTMPP in the pores is energetically disfavored but also that local intermolecular interactions (i.e., H-bonding) favor inclusion at sites necessary for pores closure to complete the network topology. This provides independent evidence for the repulsive interaction between in-pore adsorbates and the confined surface state. Despite the complexity of the structure, the molecules composing it are of only two unique conformations, one at vertices another at pore walls, whose transformations (stepwise 60° rotations) in the 2-dimensional plane can be used to generate the whole lattice. TTMPP molecules on the Ag(111) surface remain in a non-metalated state after their deposition on samples held at room temperature. This has been confirmed by in-situ X-ray photoelectron spectroscopy (XPS) results (See Supplementary Fig. 3). In the N1s XPS spectrum, there are two peaks of approximately equal intensity corresponding to imine N (398.3 eV) and pyrrolic N-H (400.4 eV) of the porphyrin macrocycle[32]. The presence of two N1s XPS peaks also indicates that tautomeric processes[33] of the exchangeable pyrrolic protons are arrested in TTMPP molecules adsorbed at the Ag(111) surface. XPS spectra of Ag(II) porphyrins are complicated by their magnetic properties although a single XPS N1s peak at 398.5 eV has been reported for Ag(II)TPP[34] (TPP = meso-tetraphenylporphyrin). Also, the high temperature annealing of TPP at 550 K on Ag(111) surface does not result in metalation of TPP to Ag(II) TPP[35].

The formation of the Kagome lattice can be assessed by considering the intermolecular regions of the molecules as observed by scanning tunneling microscopy images (see Fig. 2). Figure 2a shows individual and partly aggregated molecules not contained in the Kagome lattice structure. On Ag(111) surfaces held at room temperature, TTMPP molecules are mobile while at 5 K (temperature used for imaging) they are immobile neither forming a 2-dimensional gas phase, as is often observed for porphyrins adsorbed at metallic interfaces[36,37], nor undergoing rotational translation. Two imaging modes, which depend on the polarity of the bias voltage in the STM junction[28,38], provide more contrast of the σ (Fig. 2a,b (upper panels)) and the π (Fig. 2a,b (lower panels)) bonds of the surface supported molecules. This allows for the identification of the relative positions of different structural features within the molecules. For example, a distinct groove in the σ-imaging profile (Fig. 1a) is characteristic of macrocyclic saddling[20] (see also Supplementary Fig. 4). In this state, substituents are arranged so that methyl groups remote from the surface are proximal (emphasizing the 'groove' profile) and the pyrrole groups of the macrocycle are weakly saddled in order to disperse intramolecular steric interactions. As shown in Figs. 1c and 2b, it is convenient to describe the Kagome structure using a trimer of molecules where STM images indicate double intermolecular interactions (denoted by yellow/orange bars) between both of the terminal ('pore wall') TTMPPs and a central TTMPP (which is at the Kagome vertex). These trimers form the Kagome lattice through single interactions (denoted by red triangles) of the terminal molecules at the vacant positions of the vertex molecules (denoted by green triangles), as indicated in Fig. 1c,d (see also Supplementary Fig. 2). The two unique areas of intermolecular interactions are indicated by colored frames in Fig. 2b (lower panel). The model (Fig. 2c) constructed using space-filling molecules agrees well with the observed structure reproducing the chirality of the network (Supplementary Fig. 5) and the 60° rotational translation of the molecules in the lattice (Fig. 2c, lower panel, green lines). The form of intermolecular interactions at the vertex TTMPP molecules is reminiscent of that found in its X-ray crystal structure although the intermolecular (centroids) distance of 1.5 nm in that case compared with 2.1 nm on Ag(111) indicate that pyrrolic β-C-H…OCH_3 hydrogen bonding interactions occurring in the crystal (indicated by the red broken bonds in Fig. 2d) are not possible in the on-surface assembly (in Fig. 2d, other intermolecular H-bonds are indicated by yellow broken bonds, intramolecular H-bonds are shown by turquoise broken bonds; see also Supplementary Fig. 6). Different conformations of the TTMPP molecules at the surface also do not favor those types of intermolecular interactions. Intermolecular hydrogen bonding interactions of TTMPP on Ag(111) (highlighted in Fig. 2b) were considered by using Density Functional Theory (DFT) calculations. The results are shown in Fig. 2e,f respectively for inter-trimer H-bonding (single interaction, red/green triangles) and intra-trimer H-bonding (double interaction, yellow/orange bars); for further details see Supplementary Figs. 7 & 8; for simulated STM images of the respective intermolecular contacts see Supplementary Fig. 9. These structures show the potential H-bonding interactions occurring between molecules of TTMPP forming the Kagome lattice (red broken bonds: intermolecular; turquoise broken bonds: intramolecular). Similar interactions can also be found in the available crystal structures[29–31,39–41] of TTMPP and its metal complexes. It should be noted here that while there exists a C-H…O hydrogen bond between a pyrrole beta CH group and a methoxy group[42] of an adjacent molecule (O4…H13: 2.7848(1) Å) in the X-ray structure of TTMPP, the separation of the molecules in the on-surface structure probably precludes CH…O hydrogen bonding[43,44] in its on-surface Kagome self-assembly.

Molecular Deposition

The formation of the TTMPP Kagome structure was studied by considering different coverages of the molecules on Ag(111). As shown in Fig. 3, different coverages correspond to different surface structures, with average separation of molecule islands defined as D_{avg} (see the Table). At 0.2 Hz coverage (Fig. 3a), TTMPP molecules are visible as immobile divided molecules indicating intermolecular repulsive interactions (D_{avg} = 9.091 nm). Interestingly, there are several small dimers, trimers and triangular units present indicating that the intermolecular repulsion is not strong enough to exclude intermolecular approach, i.e., it is driven by Coulombic repulsion. At 0.3 Hz, structures suggestive of a Kagome lattice emerge (D_{avg} = 8.226 nm; Fig. 3b). At higher coverages (0.4 Hz: Fig. 3c; 0.5 Hz: Fig. 3d), extended areas of Kagome structure are clearly established on the substrate and D_{avg} = 7.031 nm (0.4 Hz) and D_{avg} = 6.226 nm (0.5 Hz). Considering values of Davg, the distances between molecular islands are not remarkably reduced as larger Kagome network patches are formed. This provides unambiguous evidence that long range interactions occur, which are tentatively assigned to Coulomb forces. There are two additional features of the molecules when deposited in a separated state (such as in Fig. 3a, b): (i) molecules are not all deposited at sites predictably to be included in the eventually formed Kagome lattice, and (ii) molecules are fixed in one of three possible states with mutual trigonal orientation as indicated by the groove feature due to the saddling of the porphyrin macrocycle. These two features imply that although the molecules are stationary, they are translated on the substrate as the lattice structure is formed, and that the underlying substrate lattice determines the relative orientations of the molecules (a situation which persists in molecules when eventually contained in the Kagome lattice). Overall, as illustrated by Fig. 3, the on-surface formation of Kagome structure is coverage dependent involving concerted molecular rearrangement on the substrate once a sufficient density of molecules is attained.

Interaction of the TTMPP Kagome Lattice with the underlying surface state

To probe the Shockley state of the Ag(111) surface at different proximities to the molecules in the Kagome structure, dI/dV spectroscopy was performed at different points (see Fig. 4). Figure 4a shows STM images indicating points in the structure (Fig. 4b shows a corresponding models) that were probed and the corresponding spectra are shown in Fig. 4c. Based on these data, it

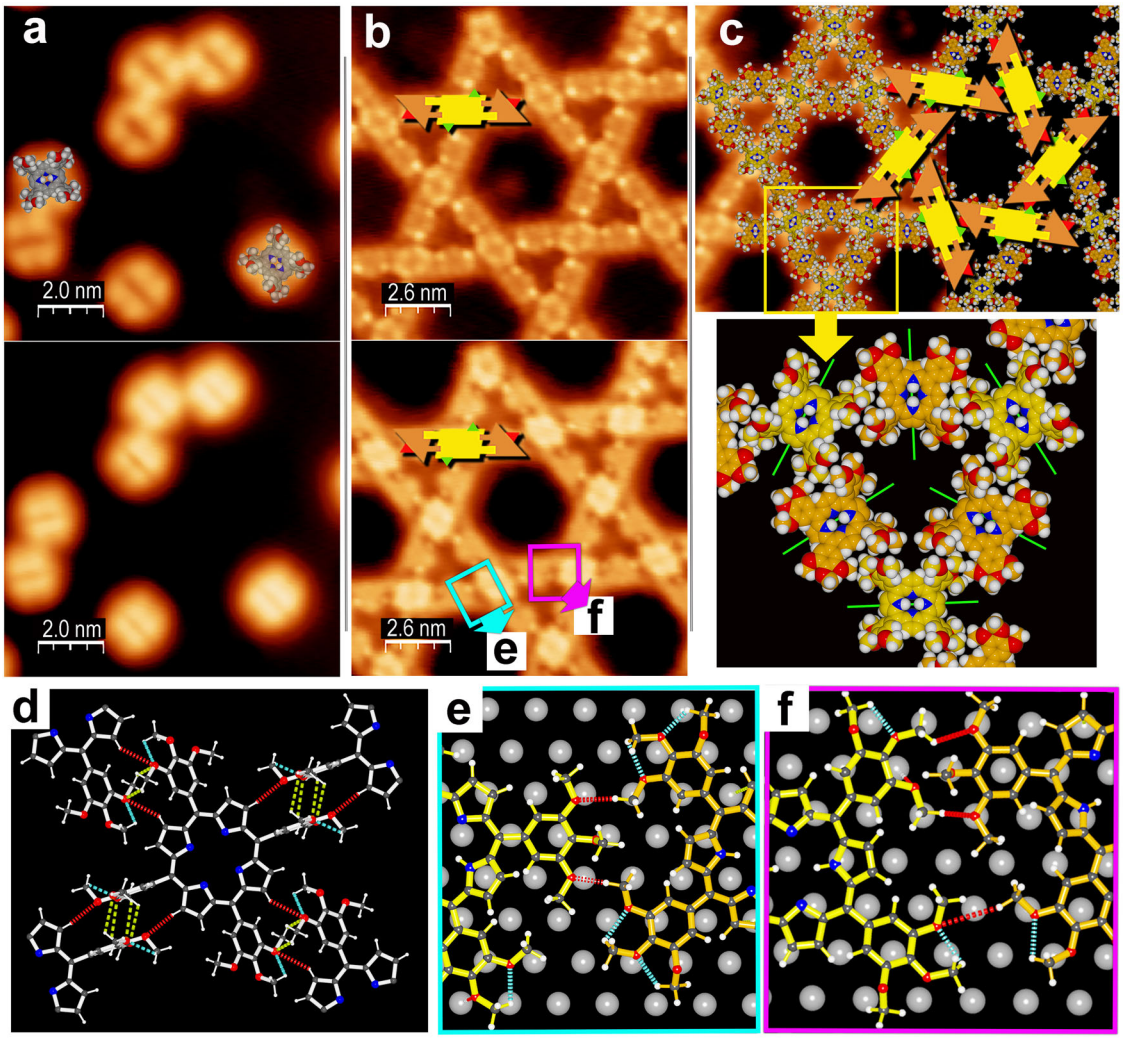

Fig. 2 | Conformation and hydrogen bonding in TTMPP. a Two STM imaging modes sensitive to σ (upper: image: 10 nm; I = 10 pA; V = 1.0 V) and π (lower: Image: 10 nm; I = 10 pA; V = –1.0 V) bonding modes are shown for TTMPP molecules not contained in Kagome formation. **b** Two STM imaging modes: σ-bonded methyl groups appear more pronounced in the upper micrograph (10 nm; I = 10 pA; V = 1.0 V) and π-orbitals of the porphyrin core appear more pronounced in the lower micrograph (10 nm; I = 10 pA; V = –1.0 V) of the Kagome structure. In the lower panel, colored frames indicate intermolecular interactions studied using DFT calculations shown in the indicated panels. **c** STM image overlaid with space-filling representations of the two unique molecular conformers established in response to the formation of the Kagome lattice on Ag(111) and an exploded view of the triangular vertex. **d** Hydrogen bonding interactions in crystals of TTMPP. A single TTMPP molecule is shown with interacting portions of four adjacent molecules. Important H-bonds: O4…H13: 2.7848(1) Å (red), O2…H27: 2.5020(1) Å, O4…H23B: 2.9563(1) Å (turquoise), O1…H10C: 2.4536(1) Å (yellow). (See also Supplementary Fig. 6). **e** Calculated (DFT) structure at the close approach of molecules with 'single' intra-trimer H-bonding interaction (see also Supplementary Fig. 7). **f** Calculated (DFT) structure at the close approach of molecules with 'double' intra-trimer H-bonding interaction (see also Supplementary Fig. 8).

can be seen that the momentum averaged density of states of the surface state shifts gradually from its free surface position at –64 meV[45] to values very close to the Fermi level (E_f) by the confinement of the probing position in the proximity of molecular structures. In the absence of the Kagome self-assembly, the value reaches –33 meV while the value at the center of the large pore structure in the Kagome shifts more significantly to just –14 meV below E_f. The gradual shifting of the surface state with increasing proximity to the adsorbed molecules (ad-molecules) reflects Pauli repulsion between the ad-molecules and the underlying surface state. The more significant shift in binding energy for points within the large pore of the Kagome lattice indicates that this network phase is substantially stabilized over the compact molecular ad-layer islands by the existence of the confined surface state. Similar shifts in dI/dV characteristics of supramolecular pore structures[46] are characteristic of so-called quantum box states (QBS) so that TTMPP molecules on Ag(111) can be considered a quantum Kagome box.

Although often found in the lattices of inorganic materials[47], Kagome networks can also emerge from planar molecules with fixed conformation of particular geometries being deposited on 2D substrates. Several different mechanisms of formation are available including those based on 'corner-to-corner' interactions (especially in planar symmetrical molecules[48,49] including porphyrins[50]), and others based on staggered assembly of high aspect ratio molecules such as oligophenylenes[51] or transition metal complexes[52,53]. While these systems generally involve homogeneous interactions involving a single type of species, diversity of interaction and molecular co-assembly may also yield Kagome-like morphologies[54,55]. The latter provide excellent examples of how regular, yet compositionally complex structures can be established, similarly to the Kagome lattice presented here, where co-assembly of conformational isomers is determined by the adaptability of the TTMPP molecule. In the present case, the unique geometrical considerations of the Kagome lattice have been combined with on-surface chirality and quantum states making it highly attractive for further study of those and other complex properties of this material system. In particular, the emergence of chirality by assembly of achiral molecules, so-called supramolecular chirality[56], is an important subject. In the case of

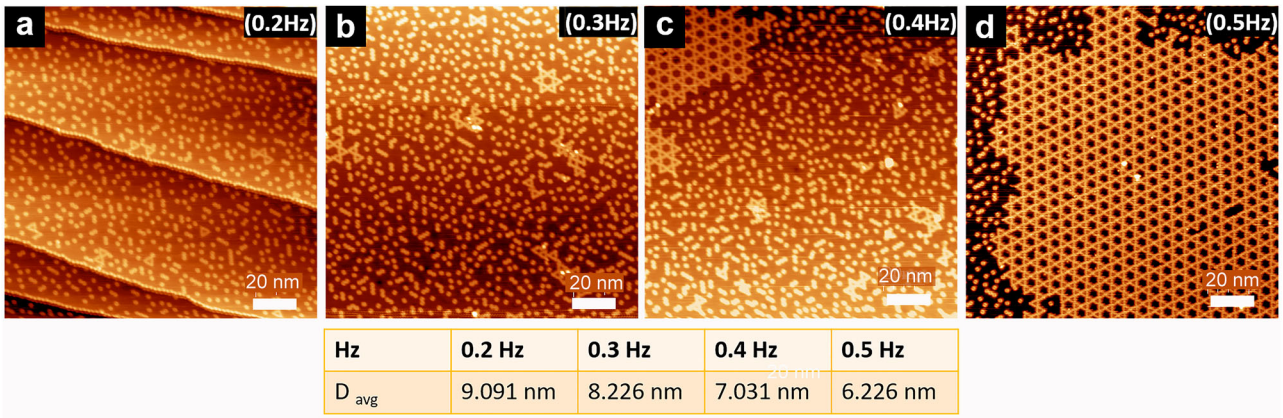

Hz	0.2 Hz	0.3 Hz	0.4 Hz	0.5 Hz
D_{avg}	9.091 nm	8.226 nm	7.031 nm	6.226 nm

Fig. 3 | Emergence of surface structure for TTMPP molecules during assembly with progressively increasing molecular coverage. a Molecular coverage = 0.2 Hz, molecules are randomly distributed indicating repulsive intermolecular interactions (D_{avg} = average distance between molecular islands). **b** Molecular coverage = 0.3 Hz – as D_{avg} is reduced with increasing coverage, some triangular units and larger star shaped assemblies are formed. **c** Molecular coverage = 0.4 Hz – larger areas of the network assembled structure appear at higher deposition rates (increased coverage). **d** Molecular coverage = 0.5 Hz – large patches of agglomerated supramolecular islands of the Kagome network topology become visible. Table: D_{avg} between molecular islands is not remarkably reduced as larger Kagome network patches are formed. This provides unambiguous evidence that long range interactions occur, which are assigned to repulsive forces. (Images obtained at 5 K: 150 × 150 nm, I = 30 pA, V = 1.5 V).

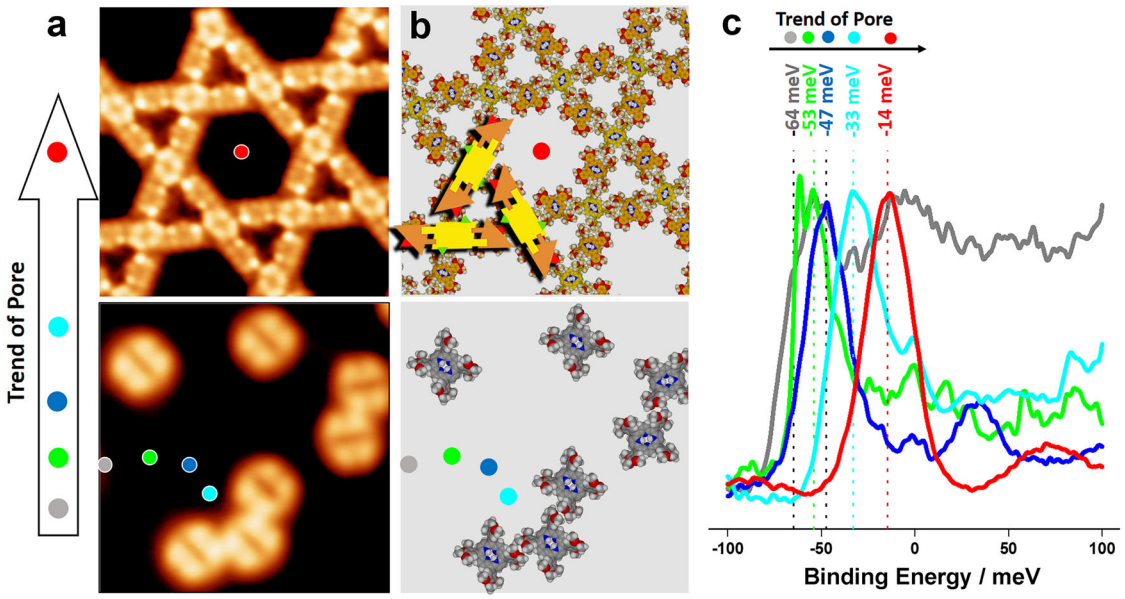

Fig. 4 | Evolution of the Ag(111) surface state from its nearly free character to a quantum well state according to molecular proximity and at the interior of pore cavities. a STM images of (top) Kagome lattice of TTMPP molecules and (bottom) non-Kagome molecules with points of binding energy measurement denoted by color-coded spots. **b** Model representations of the STM images in (**a**) indicating the trimer (upper) and space-filling structures (lower). **c** dI/dV data obtained at the points shown in (**a**).

Kagome structures, chirality emerges by different mechanisms involving molecular in-plane chirality[49,50,57], unusual intermolecular interactions[55] (including hydrogen bonding[58], similar to the case for TTMPP) or on-surface chemical reactions[59].

Discussion

The above conclusions about the complexity of the interaction potentials causing conformational diversity and forming the Kagome network on Ag(111) is further confirmed by our observation of similar, but also distinctively different supramolecular structures of TTMPP on another substrate, i.e. atomically clean Au(111). (See Fig. 5a, b) In this latter case, the formation of an extended lattice is obstructed by the corrugated herringbone structure of the Au(111) reconstruction. This leads to isolated conformers coexisting with uni- and bi-molecular chains. Also, we observe individual units of unilateral triangles closely resembling the small pore in the Kagome network. We also note that at higher 2D packing densities in certain confinements parallel chains are covering all available surface area on the facet. This underlines the tendency of TTMPP to undergo similar if not the same intermolecular interactions also on this substrate while the structures formed are laterally confined by the fcc domain of the 22 × SQRT(3) reconstruction of Au(111). This further confirms that the molecule can assume different coexisting conformations and configurations to build different topological structures by linking 2-armed and 3-armed conformers. It appears that rather weak differences of the adsorbate-adsorbent interactions in the form of the TTMPP adsorption strength on the different (fcc or hcp) domains of the surface reconstruction or in the presence or absence of the underlying surface state are guiding the conformational flexure of the conformers and the overall structure and topology of the

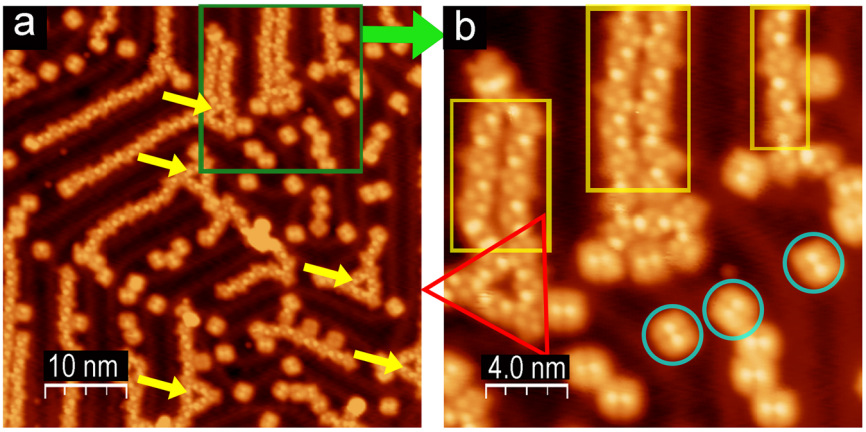

Fig. 5 | STM images of TTMPP deposited onto Au(111). a Supramolecular structures formed from TTMPP in presence of the lateral confinement experienced by its preferential adsorption on the fcc facets of the Au(111) herringbone reconstruction. Individual conformers, single chains and double chains are visible as well as some triangular pores (yellow arrows) reminiscent of one unit of the Kagome network found on Ag(111). **b** Expansion of highlighted area (green box in **a**) -of-similarity with the structures found on Ag(111): Red triangle—triangular Kagome-type vertex; yellow boxes—chains of TTMPP with meso-substituents in opposing positions having different conformations (similar to the case on Ag(111); see Supplementary Fig. 4); blue circles—individual molecules exhibiting saddle conformations.

resulting supramolecular structure, which involves only a SINGLE TYPE of molecule—the remarkable feature in this case.

The coexistence of different ligating and non-ligating conformers which we report here for TTMPP on surfaces adds to its properties as a ligand for coordination chemistry[30,32,39–41,60,61]. Several crystal structures of the complexes are available and these confirm the role of the peripheral methoxy groups in determining the molecular arrangement we observe on surfaces. The conformational flexibility of molecules is constrained by their rather strong adsorption in the surface potential compared to typical crystal fields in the state of a solid crystal or powder. Thus it is remarkable that the methoxy groups enable well-ordered Kagome networks on Ag(111) and similarly well-ordered -A-B-A-B-A- chains of different conformers on Au(111) among the other structures. Importantly, other *meso*-tetraphenylporphyrins have not been reported to form Kagome lattices on Ag(111)[35,62] indicating its unique conformational diversity that also persists in the surface adsorbed state. We attribute this to the large conformational degree of freedom of the three methoxy groups linked to each of the phenyl substituents. These are sterically demanding ("bulky") enough to reduce the considerable interaction between the porphyrin-π system and the metal substrate to a level that rotations of the phenyl-porphyrin dihedral angle can lead to a large number of conformational states with different orientations of the methoxy groups. A rather low activation barrier between different conformers facilitates their cooperative adaptation and the formation of different H-bond motifs as well as the formation of large supramolecular islands, which is also determined by modulations of the surface potential and/or the higher or lower electron density of the surface states. Also, this low activation barrier allows for the inter-conversion of molecular conformers which leads to the rare presence of "trapped" molecules in the Kagome network as mentioned above. It is worth noting that low activation barriers for conformational adaptations in conjunction with complex conformational degrees of freedom of phenoxy substituents of a phthalocyanine have also been identified to cause of the complex phase evolution observed with increasing packing density on Ag(111)[63].

While there are many molecular modules assembling by homogeneous intermolecular interactions[64–67], the combined action of intra- and intermolecular processes[68,69] including hydrogen bonding, can become a significant structure-controlling factor towards increasingly complex self-assemblies at surfaces[70,71]. For TTMPP, it is the excellent stability, adaptable conformation and available multiple hydrogen bond donors/acceptors (methoxy groups) that are critical factors in the present case. The remarkable observation of conformational diversity should also be discussed in thermodynamic terms[13]: the most energetically favored conformational state of an *individual* molecule—AND its substrate-specific adaptation as an isolated adsorbate clearly differs from the in-chain states and the Kagome network/triangle states on any of the substrates studied. Thus, the supramolecular assembly is not formed by conformers that have been stabilized in two different configurations by surface adsorption as is the typical case for substituted pro-chiral porphyrins assuming one or the other conformation/chirality prior to their assembly into a binary structure of conformers. In the present case, it is rather the cooperative action of all available forces—including the nearest-neighbor interactions—which leads to the observed phenomena.

The main lesson to be learned from our report is not simply the observation of a self-assembled Kagome lattice. Similar lattices have been found in 3D and 2D aggregates of a broad range of molecular components[72–77], and have shown exciting structure-dependent properties including magnetism and superconductivity[78,79]. What makes the present system so peculiar is the emergence of a rather complex supramolecular structure by dynamic conformational adaptation as molecules interact with their counterparts under different external constraints. This concept, while ubiquitous in nature, is to the best of our knowledge new for on-surface supramolecular assemblies where molecular modules assemble and re-assemble after having assumed their on-surface conformational state. It appears that the induced-fit concept[80,81] describing the interlocking of biomolecules during the formation of a supramolecular structure or upon recognition of an enzymatic site can be mimicked by the behavior of a single and relatively small molecule on a surface. Notably also, the present work renders it plausible that simple molecules with sufficient conformational degrees of freedom interacting with interfaces might have contributed to the emergence of early supramolecular systems at early stages of prebiotic systems. The accumulation of molecular modules and their spontaneous integration into supramolecular structures at, for instance, clay or membrane/micelle interfaces[1,82] is an interesting concept that has been recognized for its potential importance and which should be investigated further in the context of any interactions with conformationally flexible molecules.

Methods

General

All chemicals and solvents used in the synthesis of TTMPP were obtained from Tokyo Kasei Chemical Co. Ltd., Wako Chemical Co. Ltd., Nacalai Tesque Chemical Co. Ltd or Sigma-Aldrich Chemical Co. Ltd and were used as received without further purification. TTMPP was prepared and purified as previously reported[83,84]. Further purification was performed by recrystallization where a solution of the porphyrin in dichloromethane was layered with a similar volume of *n*-hexane. Crystals suitable for X-ray crystallography were also prepared by this method.

X-ray crystallography

Crystals of TTMPP were grown by layering hexane onto a solution of the porphyrin in dichloromethane. Large diffraction quality crystals grew over the course of 2–3 days. Data collection was performed using MoKα radiation (λ = 0.71073 Å) on a RIGAKU VariMax Saturn diffractometer equipped with a charge-coupled device (CCD) detector. Prior to the diffraction experiment, the crystal was flash-cooled to 113 K in a stream of cold

nitrogen gas. Cell refinements and data reductions were carried out using the d*trek program package in the CrystalClear software suite[85]. The structures were solved using a dual-space algorithm method (SHELXT)[86] and refined by full-matrix least squares on F2 using SHELXL-2014[87] in the WinGX program package[88]. Non-hydrogen atoms were anisotropically refined and hydrogen atoms were placed on calculated positions with temperature factors fixed at 1.2 times Ueq of the parent atoms and 1.5 times Ueq for methyl groups. Crystallographic data (excluding structure factors) have been deposited with the Cambridge Crystallographic Data Centre with CCDC reference number 2091153 (TTMPP) Copies of the data can be obtained, free of charge, on application to CCDC, 12 Union Road, Cambridge CB2 1EZ, UK http://www.ccdc.cam.ac.uk/perl/catreq/catreq.cgi, e-mail: data request@ ccdc.cam.ac.uk, or fax: +44 1223 336033.

Scanning tunneling microscopy

All imaging experiments were performed using an Omicron low temperature STM operating at 4.8 K in ultrahigh vacuum (UHV). Clean Ag(111) and Au(111) surfaces were prepared in-situ by repeated cycles of sputtering and annealing. Mechanically sharpened and sputter-etch cleaned PtIr tips were used. All sample preparations were performed under ultrahigh vacuum (UHV) conditions with a base pressure of $\sim 10^{-10}$ mbar. The crystals were cleaned using cycles of sputtering with Ar^+ ions with subsequent annealing at 450 °C. Thermal evaporation at 300 °C was used to deposit the molecules using a commercial evaporator (Kentax GmbH, Germany) onto the substrate maintained at room temperature. The sublimed amounts of the compounds were controlled by using a quartz crystal microbalance positioned in similar distance from the source like the sample during the exposure. The molecular coverage has been given in Hz, i.e. the frequency shift by the accumulated mass on the quartz oszillator. STM imaging was performed in constant current mode (typical tunneling current 10–50 pA) with the selected sample bias in the range of 3 mV to 1 V at 5 K. Pt-Ir wires (90% Pt, 10% Ir) were used to make scanning probe tips and these were cleaned by sputtering with Ar^+ ions prior to use.

X-ray photoelectron spectroscopy

In order to rule out that the observed supramolecular arrangements had not been caused by Ag coordination through the methoxy ligands, XPS experiments have been performed. These experiments were performed using a SPECS XR50 M Al Kα excitation source emitting X-rays at 1486.7 eV monochromatized using a SPECS FOCUS 500 quartz single crystal mirror monochromator. The kinetic energy of the photoelectrons had been analyzed with a PHOIBOS 150 electron energy analyzer and counted with a 1D delay line detector (1D DLD). N1s XPS Spectra have been acquired for the Ag(111) substrate, and after deposition of (1) close to a monolayer of the TTMPP molecules, (2) about twice this amount and (3) a multilayer as estimated by using a Quartz Crystal Microbalance (QCMB). Long acquisition times (~12 h) were required for both the reference measurements of the clean substrate and for the molecular layers in order to obtain meaningful spectra and useful data were acquired despite the coincidence of the N1s XPS line with a plasma resonance in the Ag substrate as has been reported previously by Rieger et al[89].

Density functional theory calculations

The DFT calculations were performed using the Siesta code[90–92]. This uses norm-conserving pseudopotentials[93] and expands the wave functions of valence electrons in LCAO form. As exchange-correlation functional, we have used the vdW-DF-cx functional of Berland and Hyldgaard (BH)[94]. The silver surfaces were constructed based on the bulk parameter of 4.078 Å. The geometric systems were confined to unit cells that allow the study of periodically repeating Ag(111) surface; the super-cell include $10 \times 10 \times 3$ silver atoms for single molecule calculations and $15 \times 15 \times 3$ atoms for the dimer calculations. To avoid the spurious contribution of the neighbor cell over the molecule (i.e. artificial influence of the electric charge from one cell to another), the length of the cells along the OZ axis was set to 30 Å for all the systems studied, with a vacuum level of ~20 Å. We used double-zeta polarized (DZP) basis sets with an energy shift of 150 meV for all atoms. The relaxation procedure is based on the Conjugated Gradient method. The systems were relaxed by keeping the silver substrate pinned at their bulk positions, only the molecule being permitted to relax until the maximum gradient in the structure was below 0.05 eV/A. Other calculations were performed using the Gaussian 16 program[95], and the results were analyzed and visualized on GaussView 6. Geometry optimization was performed at the density functional theory (DFT) level with the B3LYP functional, the gradient correction of the exchange functional by Becke[96,97] and the correlation functional by Lee, Yang and Parr[98], and the 6–31 G(d,p) split valence was used.

Interaction energy

The interaction energy (with basis set superposition error corrections) between molecules and surface, ΔE, is defined as the difference between the total energy of the molecule–surface composite and the sum of the energies of the molecule and the surface. When the surface energy is calculated, we atoms of the molecule are considered 'ghost' atoms, while for molecular energy calculations, the atoms of the surface are treated as ghost atoms.

Charge transfer

Charge transfer between surface and molecules, and between molecules of the dimer can be estimated from the spatially resolved charge-density difference, defined as $\Delta\rho(\vec{r}) = \rho_{total}(\vec{r}) - [\rho_{mol}(\vec{r}) + \rho_{surf}(\vec{r})]$, where $\rho_{total}(\vec{r})$, $\rho_{mol}(\vec{r})$ and $\rho_{surf}(\vec{r})$ are the (negative) charge densities of the relaxed adsorbate−substrate system (total), adsorbate without substrate (mol), and clean surface (surf), respectively. Starting from this equation, we can estimate the molecule−surface charge transfer and the formation of the interface dipoles. The methodology used for charge transfer calculations has been described comprehensively in our previous benchmark paper[99].

Simulations of the STM images

Were performed by using the Tersoff-Hamman approximation (i.e. STM image is determined by the local density of states (LDOS)[100]). We computed LDOS in the energy window spanning from the Fermi level of the system up to 1 eV below the Fermi level, corresponding to an external bias of 1 V. We scanned the surface by searching for a given constant value of the LDOS (i.e. we simulate a constant current STM experiment).

Data availability

Crystallographic data (excluding structure factors) have been deposited with the Cambridge Crystallographic Data Centre with CCDC reference number 2091153 (TTMPP). Copies of the data can be obtained, free of charge, on application to CCDC, 12 Union Road, Cambridge CB2 1EZ, UK http://www.ccdc.cam.ac.uk/perl/catreq/catreq.cgi, e-mail: data_request@ ccdc.cam.ac.uk, or fax: +44 1223 336033. CIF file for TTMPP is supplied as Supplementary Data 1 (Checkcif—Supplementary Data 2). Atomic coordinates of optimized structures are supplied as Supplementary Data 3, 4 and 5.

Received: 8 May 2025; Accepted: 10 July 2025;
Published online: 24 July 2025

References

1. Ruiz-Mirazo, K., Briones, C. & de la Escosura, A. Prebiotic systems chemistry: new perspectives for the origins of life. *Chem. Rev.* **114**, 285–366 (2014).
2. Lazcano, A. & Miller, S. L. The origin and early evolution of life: prebiotic chemistry, the pre-RNA world, and time. *Cell* **85**, 793–798 (1996).
3. Chandler, D. Interfaces and the driving force of hydrophobic assembly. *Nature* **437**, 640–647 (2005).
4. Ianiro, A. et al. Liquid-liquid phase separation during amphiphilic self-assembly. *Nat. Chem.* **11**, 320–328 (2019).

5. Ciesielski, A., Palma, C.-A., Bonini, M. & Samori, P. Towards supramolecular engineering of functional nanomaterials: pre-programming multi-component 2D self-assembly at solid-liquid interfaces. *Adv. Mater.* **22**, 3506–3520 (2010).
6. Yang, H., Yuan, B., Zhang, X. & Scherman, O. A. Supramolecular chemistry at interfaces: host-guest interactions for fabricating multifunctional biointerfaces. *Acc. Chem. Res.* **47**, 2106–2115 (2014).
7. Bickerton, L. F., Johnson, T. G., Kerckhoffs, A. & Langton, M. J. Supramolecular chemistry in lipid bilayer membranes. *Chem. Sci.* **12**, 11252–11274 (2021).
8. Junge, W. & Nelson, N. ATP synthase. *Ann. Rev. Biochem.* **84**, 631–657 (2015).
9. Robert-Paganin, J., Pylypenko, O., Kikuti, C., Sweeney, H. L. & Houdusse, A. Force generation by myosin motors: a structural perspective. *Chem. Rev.* **120**, 5–35 (2020).
10. Schliwa, M. & Woehlke, G. Molecular motors. *Nature* **422**, 759–765 (2003).
11. Stoddart, J. F. Mechanically interlocked molecules (MIMs)—molecular shuttles, switches, and machines (Nobel lecture). *Angew. Chem. Int. Ed.* **56**, 11094–11125 (2017).
12. Kasem, S. et al. Artificial molecular motors. *Chem. Soc. Rev.* **46**, 2593–2621 (2017).
13. Singh, A., Parvin, P., Saha, B. & Das, D. Non-equilibrium self-assembly for living matter-like properties. *Nat. Rev. Chem.* **8**, 729–740 (2024).
14. Maclean, O. & Rosei, F. Two-dimensional polymers grow up. *Science* **366**, 1308–1309 (2019).
15. Moradi, M. et al. Supramolecular architectures of molecularly thin yet robust free-standing layers. *Sci. Adv.* **5**, eaav4489 (2019).
16. Auwaerter, W., Ejica, D., Klappenberger, F. & Barth, J. V. Porphyrins at interfaces. *Nat. Chem.* **7**, 105–120 (2015).
17. Meng, T., Lei, P. & Zeng, Q. Progress in the self-assembly of porphyrin derivatives on surfaces: STM reveals. *New. J. Chem.* **45**, 15739–15747 (2021).
18. Iacovita, C. et al. Controlling the dimensionality and structure of supramolecular porphyrin assemblies by their functional substituents: dimers, chains, and close-packed 2D assemblies. *Chem. Eur. J.* **18**, 14610–14613 (2012).
19. Drain, C. M., Varotto, A. & Radivojevic, I. Self-organized porphyrinic materials. *Chem. Rev.* **109**, 1630–1658 (2009).
20. Jung, T., Schlittler, R. & Gimzewski, J. Conformational identification of individual adsorbed molecules with the STM. *Nature* **386**, 696–698 (1997).
21. Loppacher, C. H. et al. Direct determination of the energy required to operate a single molecule switch. *Phys. Rev. Lett.* **90**, 066107 (2003).
22. Jirásek, M., Anderson, H. L. & Peeks, M. D. From macrocycles to quantum rings: does aromaticity have a size limit?. *Acc. Chem. Res.* **54**, 3241–3251 (2021).
23. Ishihara, S. et al. Porphyrin-based sensor nanoarchitectonics in diverse physical detection mode. *Phys. Chem. Chem. Phys.* **16**, 9713–9746 (2014).
24. Ding, Y., Zhu, W.-H. & Xie, Y. Development of ion chemosensors based on porphyrin analogues. *Chem. Rev.* **117**, 2203–2256 (2017).
25. Kadish, K. M., Smith, K. M. & Guilard, R. (eds.) *Handbook of Porphyrin Science,* Vol. 10 (World Scientific, 2010).
26. Yokoyama, T., Kamikado, T., Yokoyama, S. & Mashiko, S. Conformation selective assembly of carboxyphenyl substituted porphyrins on Au (111). *J. Chem. Phys.* **121**, 11993–11997 (2004).
27. Zhang, Q. et al. Single-molecule investigations of conformation adaptation of porphyrins on surfaces. *J. Phys. Chem. Lett.* **8**, 1241–1247 (2017).
28. Wintjes, N. et al. Supramolecular synthons on surfaces: controlling dimensionality and periodicity of tetraarylporphyrin assemblies by the interplay of cyano and alkoxy substituents. *Chem. Eur. J.* **14**, 5794–5802 (2008).
29. Jiao, X.-D. et al. Crystal and molecular structure of meso-5,10,15,20-tetra(3,4,5-trimethoxyphenyl)porphyrin. *Jiegou Huaxue* **15**, 205–209 (1996).
30. Yang, N. et al. Inhibition of SARS coronavirus helicase by bismuth complexes. *Chem. Commun*. **42**, 4413–4415 (2007)
31. Bhuyan, J. & Sarkar, S. Self-assembly of magnesium and zinc trimethoxyphenylporphyrin polymer as nanospheres and nanorods. *Cryst. Growth Des.* **11**, 5410–5414 (2011).
32. Gottfried, J. M., Flechtner, K., Kreschmann, A., Lukasczyk, T. & Steinrück, H.-P. Direct synthesis of a metalloporphyrin complex on a surface. *J. Am. Chem. Soc.* **128**, 5644–5646 (2006).
33. Storm, C. B. & Teklu, Y. Nitrogen-hydrogen tautomerism in porphyrines and chlorines. *J. Am. Chem. Soc.* **94**, 1745–1747 (1972).
34. Karweik, D. H. & Winograd, N. Nitrogen charge distributions in free-base porphyrins, metalloporphyrins, and their reduced analogs observed by X-ray photoelectron spectroscopy. *Inorg. Chem.* **15**, 2336–2342 (1976).
35. Di Santo, G. et al. Supramolecular engineering through temperature-induced chemical modification of 2H-tetraphenylporphyrin on Ag(111): flat phenyl conformations and possible dehydrogenation reactions. *Chem. Eur. J.* **17**, 14354–14359 (2011).
36. Schunak, M. et al. Long jumps in the surface diffusion of large molecules. *Phys. Rev. Lett.* **88**, 156102 (2002).
37. Edmondson, M. & Saywell, A. Molecular diffusion and self-assembly: quantifying the influence of substrate hcp and fcc atomic stacking. *Nano Lett.* **22**, 8210–8215 (2022).
38. Weigelt, S. et al. Chiral switching by spontaneous conformational change in adsorbed organic molecules. *Nat. Mater.* **5**, 112–117 (2006).
39. Hibbs, W., Arif, A. M., Botoshansky, M., Kaftory, M. & Miller, J. S. Structure and magnetic properties of tetraarylporphinatomagnesium(II) electron transfer salts of 2,3,5,6-tetrafluoro-7,7,8,8-tetracyanoquinodi methane, $TCNQF_4$. *Inorg. Chem.* **42**, 2311–2322 (2003).
40. Wong, S.-Y., Sun, R. W.-Y., Chung, N. P.-Y., Liu, C.-L. & Che, C.-M. Physiologically stable vanadium(IV) porphyrins as a new class of anti-HIV agents. *Chem. Commun.* **2005**, 3544–3546 (2005).
41. Wong, W.-K. et al. Synthesis, structure and near-infrared luminescence of neutral 3d-4f bi-metallic monoporphyrinoid complexes. *J. Chem. Soc. Dalton Trans.* **2002**, 3092–3098 (2001).
42. Veljković, D. Ž, Janjić, G. V. & Zarić, S. D. Are C-H…O interactions linear? The case of aromatic CH donors. *CrystEngComm* **13**, 5005–5010 (2011).
43. Gu, Y., Kar, T. & Scheiner, S. Fundamental properties of the CH…O interaction: Is it a true hydrogen bond?. *J. Am. Chem. Soc.* **121**, 9411–9422 (1999).
44. Desiraju, G. The C-H…O hydrogen bonds: structural implications and supramolecular design. *Acc. Chem. Res.* **29**, 441–449 (1996).
45. Reinert, F., Nicolay, G., Schmidt, S., Ehm, D. & Hüfner, S. Direct measurements of the L-gap surface states on the (111) face of noble metals by photoelectron spectroscopy. *Phys. Rev. B Condens. Matter Mater. Phys.* **63**, 115415 (2001).
46. Nowakowska, S. et al. Adsorbate-induced modification of the confining barriers in a quantum box array. *ACS Nano* **12**, 768–778 (2018).
47. Wang, Y., Wu, H., McCandless, G. T., Chan, J. Y. & Ali, M. N. Quantum states and intertwining phases in kagome materials. *Nat. Rev. Phys.* **5**, 635–658 (2023).
48. Yu, H., Jing, Y. & Heine, T. Physics and chemistry of two-dimensional triangulene-based lattices. *Acc. Chem. Res.* **58**, 61–72 (2025).
49. Pan, W.-C. et al. Diboraperylene diborinic acid self-assembly on Ag(111) – kagome flat band localized states imaged by scanning

tunneling microscopy and spectroscopy. *Angew. Chem. Int. Ed.* **63**, e202400313 (2024).
50. Adhikari, R. et al. Self-assembled 2D-coordination kagome, quadratic, and close-packed hexagonal lattices formed from a cyano-functionalized benzoporphyrin on Cu(111). *J. Phys. Chem. C.* **125**, 7204–7212 (2021).
51. Schlickum, U. et al. Chiral kagomé lattice from simple ditopic molecular bricks. *J. Am. Chem. Soc.* **130**, 11778–11782 (2008).
52. Wang, X. et al. Impact of potassium doping on a two-dimensional kagome organic framework on Ag(111). *J. Phys. Chem. Lett.* **16**, 209–214 (2025).
53. Zheng, T. et al. Synthesis of the two-dimensional robust kagome lattice on Au(111) via the introduction of Fe Atoms. *J. Phys. Chem. C.* **126**, 12009–12014 (2022).
54. Theobald, J. A. et al. Controlling molecular deposition and layer structure with supramolecular surface assemblies. *Nature* **424**, 1029–1031 (2003).
55. Beniwal, S. et al. Kagome-like lattice of a π-π stacked 3-hydroxyphenalenone on Cu(111). *Chem. Commun.* **50**, 8659–8662 (2014).
56. Liu, M., Zhang, L. & Wang, T. Supramolecular chirality in self-assembled systems. *Chem. Rev.* **115**, 7304–7397 (2015).
57. Fang, Y., Tahara, K., Ivasenko, O., Tobe, Y. & De Feyter, S. Structural insights into the mechanism of chiral recognition and chirality transfer in host-guest assemblies at the solid-liquid interface. *J. Phys. Chem. C.* **122**, 8228–8245 (2018).
58. Wang, J. et al. Constructing and transferring two-dimensional tessellation Kagome lattices via chemical reactions on Cu(111) surface. *J. Phys. Chem. Lett.* **12**, 8151–8156 (2021).
59. Wang, T. et al. Chiral Kagome lattices from on-surface synthesized molecules. *ChemPhysChem* **18**, 3329–3333 (2017).
60. Holzer, N. et al. Antimony(+5) ion induced tunable intramolecular charge transfer in hypervalent antimony(V) porphyrins. *Dalton Trans.* **51**, 5890–5903 (2022).
61. Leung, S. K.-Y., Huang, J.-S., Liang, J.-L., Che, C.-M. & Zhou, Z.-Y. Nitrido ruthenium porphyrins: synthesis, characterization, and amination reactions with hydrocarbon or silyl enol ethers. *Angew. Chem. Int. Ed.* **42**, 340–343 (2003).
62. Shubina, T. E. et al. Principle and mechanism of direct porphyrin metalation: joint experimental and theoretical investigation. *J. Am. Chem. Soc.* **129**, 9476–9483 (2007).
63. Samuely, T. et al. Two-dimensional multiphase behavior induced by sterically hindered conformational optimization of phenoxy-substituted phthalocyanines. *J. Phys. Chem. C.* **112**, 6139–6144 (2008).
64. Yokoyama, T., Yokoyama, S., Kamikado, T. & Mashiko, S. Nonplanar adsorption and orientational ordering of porphyrin molecules on Au(111). *J. Chem. Phys.* **115**, 3814–3818 (2001).
65. Auwärter, W. et al. Self-assembly and conformation of tetrapyridyl-porphyrin molecules on Ag(111). *J. Chem. Phys.* **124**, 194–708 (2006).
66. Ma, C. et al. Self-assembly of a flexible porphyrin derivative containing tert isophthalic acids and host-guest interaction at the liquid/solid interface. *J. Phys. Chem. C.* **124**, 23237–23242 (2020).
67. Blunt, M. O. et al. Controlling the two dimensional self-assembly of functionalized porphyrins via adenine-thymine quartet formation. *J. Phys. Chem. C.* **122**, 26060–26079 (2018).
68. Sun, Q. et al. Inducing open-shell character in porphyrins through surface-assisted phenalenyl π-extension. *J. Am. Chem. Soc.* **142**, 18109 (2020).
69. Baljozović, M., Pijeat, J., Campidelli, S. & Ernst, K.-H. Planar and curved π-extended porphyrins by on-surface cyclodehydrgenation. *J. Am. Chem. Soc.* **146**, 34600–34608 (2024).
70. Matena, M. et al. Conformation-controlled networking of H-bonded assemblies on surfaces. *Chem. Commun.* **45**, 3525–3527 (2009).
71. Schmidt, N. et al. Coverage-controlled polymorphism of H-bonded networks on Au(111). *J. Phys. Chem. C.* **123**, 7151–7157 (2019).
72. Shi, Z. & Lin, N. Porphyrin-based two-dimensional coordination Kagome lattice self-assembled on a Au(111) surface. *J. Am. Chem. Soc.* **131**, 5376–5377 (2009).
73. Hill, J. P., Wakayama, Y., Akada, M. & Ariga, K. Self-assembly structures of a phenol-substituted porphyrin in the solid state: hydrogen bonding, Kagomé lattice and defect tolerance. *J. Phys. Chem. C.* **111**, 16174–16180 (2007).
74. Mao, J. et al. Tunability of supramolecular Kagome lattices of magnetic phthalocyanines using graphene-based Moiré patterns as templates. *J. Am. Chem. Soc.* **131**, 14136–14137 (2009).
75. Jing, Y. & Heine, T. Two-dimensional Kagome lattices made of hetero triangulenes are Dirac semimetals or single-band semiconductors. *J. Am. Chem. Soc.* **141**, 743–747 (2019).
76. Kumar, D. et al. Manifestation of strongly correlated electrons in a 2D Kagome metal-organic framework. *Adv. Func. Mater.* **31**, 2106474 (2021).
77. Wang, X.-B. et al. A p-orbital honeycomb-Kagome lattice realized in a two-dimensional metal-organic framework. *Commun. Chem.* **6**, 73 (2023).
78. Pati, S. K. & Rao, C. N. R. Kagome network compounds and their novel magnetic properties. *Chem. Commun.* **39**, 4683–4693 (2008).
79. Deng, H. et al. Chiral kagome superconductivity modulations with residual Fermi arcs. *Nature* **632**, 775–781 (2024).
80. Koshland, D. E. The key-lock theory and the induced fit theory. *Angew. Chem. Int. Ed.* **33**, 2375–2378 (1994).
81. Ahsan, A. et al. Induced fit and mobility of cycloalkanes within nanometer-sized confinements at 5 K. *J. Phys. Chem. Lett.* **13**, 7504–7513 (2022).
82. Cleaves, H. J. Prebiotic chemistry: what we know, what we don't. *Evol. Educ. Outreach* **5**, 342–360 (2012).
83. Adler, A. D. et al. A simplified synthesis of meso-tetraphenylporphyrin. *J. Org. Chem.* **32**, 476 (1967).
84. Rousseau, K. & Dolphin, D. A purification of meso-tetraphenylporphyrin. *Tetrahedron Lett.* **15**, 4251–4254 (1974).
85. *CrystalClear* 1.3.6 by Rigaku Corporation. Software for X-ray crystallography refinement. (Rigaku Corporation, Akishima, Tokyo, Japan, 2005).
86. Sheldrick, G. M. *SHELXT*—integrated space-group and crystal-structure determination. *Acta Cryst.* **A71**, 3–8 (2015).
87. Sheldrick, G. M. A short history of *SHELX*. *Acta Cryst.* **A64**, 112–122 (2008).
88. Farrugia, L. J. *WinGX* suite for small-molecule single-crystal crystallography. *J. Appl. Cryst.* **32**, 837–838 (1999).
89. Rieger, A., Schnidrig, S., Probst, B., Ernst, K.-H. & Wäckerlin, C. Identification of on-surface reaction mechanism by targeted metalation. *J. Phys. Chem. C.* **121**, 27521–27527 (2017).
90. Ordejón, P., Artacho, E. & Soler, J. M. Self-consistent order-N density functional calculations for very large systems. *Phys. Rev. B* **53**, R10441–R10444 (1996).
91. Soler, J. M. et al. The SIESTA method for ab initio order-N materials simulations. *J. Phys.:Condens. Matter* **14**, 2745–2779 (2002).
92. Siesta: A first-principles simulation code using DFT. Current version: SIESTA 5.4.0. See the Siesta distribution site. https://launchpad.net/siesta (accessed 22 July 2025).
93. Troullier, N. & Martins, J. L. Structure and electronic properties of C_{60}. *Phys. Rev. B* **46**, 1754–1765 (1992).
94. Berland, K. & Hyldgaard, P. Exchange functional that tests the robustness of the plasmon description of the van der Waals density functional. *Phys. Rev. B* **89**, 035412 (2014).
95. Frisch, M. J. et al. *Gaussian 16, Revision C.01* (Gaussian, Inc., 2016).
96. Becke, A. D. Density-functional exchange-energy approximation with correct asymptotic behavior. *Phys. Rev. A* **38**, 3098–3100 (1988).

97. Becke, A. D. Density-functional thermochemistry. III. The role of exact exchange. *J. Chem. Phys.* **98**, 5648–5652 (1993).
98. Lee, C., Yang, W. & Parr, R. G. Development of the Colle-Salvetti correlation-energy formula into a functional of the electron density. *Phys. Rev. B* **37**, 785–789 (1988).
99. Buimaga-Iarinca, L. & Morari, C. Adsorption of small molecules on gold: a DFT localized basis set study including van der Waals effects. *Theor. Chem. Acc.* **133**, 1502 (2014).
100. Tersoff, J. & Hamann, D. R. Theory of the scanning tunneling microscope. *Phys. Rev. B* **31**, 805–813 (1985).

Acknowledgements

The authors gratefully acknowledge Prof. C. Waeckerlin for interesting and helpful discussions on the XPS analysis of sub-monolayer layers compromised by unfavorable backgrounds. This work was partly supported by World Premier International Research Center Initiative (WPI Initiative), MEXT, Japan. The authors are also grateful to JST-ERATO Yamauchi Materials Space-Tectonics Project (JPMJER2003) and the Queensland Node of the Australian National Fabrication Facility (ANFF-Q). The authors are also grateful to the Paul Scherrer Institute, the Physics Department of the University of Basel and the Swiss Nanoscience Institute, the Swiss National Science Foundation (Grant # 200020_162512, 206021_144991, 206021_121461), the Swiss Commission for Technology and Innovation (CTI, 16465.1 PFNM-NM) and the Swiss Government Excellence Scholarship Program for Foreign Scholars. L.B.-I. and C.M. acknowledge financial support from MCI Romania, CORE program, project PN23 24 01. Some of the calculations reported in this study (molecular orbital structures using Gaussian 16) were performed on the Numerical Materials Simulator at National Institute for Materials Science, Tsukuba, Japan.

Author contributions

S.F.M. performed STM measurements and processed the data. A.A. undertook STM and STS experiments, and collated data. N.D.K. and A.O. acquired and analyzed the XPS data. Y.M. performed X-ray crystallography, L.B.-I. and C.M. performed computational analyses of the on-surface structures; W.N. performed DFT computations on TTMPP molecules in the gas phase; K.A. analyzed data and supervised the work; Y.W. contributed to STM measurements; Y.Y. analyzed data and supervised; T.A.J. conceptualized the project and supervised the microscopy and tunneling spectroscopy as well as the X-ray photoelectron spectroscopy; J.P.H. synthesized and purified TTMPP, analyzed data and iteratively discussed with T.A.J. towards the consolidation and refinement of the analysis and the conclusions. Both have interacted in the final manuscript initially assembled from parts written by S.F.M. and A.A. and wrote the paper. All the authors discussed the project and contributed to the writing and preparation of the final manuscript.

Competing interests

The authors declare no competing interests.

Additional information

Supplementary information The online version contains supplementary material available at https://doi.org/10.1038/s42004-025-01607-x.

Correspondence and requests for materials should be addressed to Thomas A. Jung or Jonathan P. Hill.

Peer review information *Communications Chemistry* thanks the anonymous reviewers for their contribution to the peer review of this work.